

Spin transport properties in a naphthyl diamine derivative film investigated by the spin pumping

Yuichiro Onishi¹, Yoshio Teki^{2,3}, Eiji Shikoh^{1,3,a)}

¹*Graduate School of Engineering, Osaka City University, 3-3-138 Sugimoto, Sumiyoshi-ku,
Osaka 558-8585, Japan*

²*Graduate School of Science, Osaka City University, 3-3-138 Sugimoto, Sumiyoshi-ku, Osaka
558-8585, Japan*

³*Graduate School of Engineering, Osaka Metropolitan University, 3-3-138 Sugimoto,
Sumiyoshi-ku, Osaka 558-8585, Japan*

We report the spin transport properties in a thermally evaporated naphthyl diamine derivative (*N,N'*-Bis(naphthalen-1-yl)-*N,N'*-bis(phenyl)-2,2'-dimethylbenzidine: α -NPD) molecular thin film investigated by the spin pumping. In a palladium(Pd)/ α -NPD/Ni₈₀Fe₂₀ tri-layer structure sample, a pure spin current is generated in the α -NPD layer by the spin pumping driven by the ferromagnetic resonance of the Ni₈₀Fe₂₀ layer. The spin current is absorbed into the Pd layer, converted into a charge current with the inverse spin-Hall effect in Pd, and detected as an electromotive force. This is clear evidence for the spin transport in an α -NPD film at room temperature (RT). The spin diffusion length in an α -NPD film has been estimated to be about 62 nm at RT, which is usable as a spin transport material for developing spintronic devices.

^{a)}E-mail: shikoh@omu.ac.jp (E. Shikoh)

Pure spin current which is a flow of spin angular momenta is a dissipation-less information propagation method in electronic devices, and considered as an energy-saving technology. To utilize the pure spin current for spintronic devices, long distance spin transport and precise control of the spin current flow are needed. In *n*-type silicon (Si), the spin transport was achieved¹ and the spin current was successfully controlled with an electrical voltage.² That is, a Si-based spin transistor³ has been developed and demonstrated, where the spin current is controlled by a so-called gate voltage. Meanwhile, to control the spin current in materials with other external fields is interesting, for example, by light irradiation, heat, pressure, and so on.

Organic molecular materials which are composed of light elements are promising candidates for the spin transport materials because the spin-orbit interaction working as a spin scattering center is generally weak. Also, many molecular materials show photoconductivity for visible light (for example, pentacene thin films⁴), where the spin transport properties of molecular films can be controlled through light irradiation. In cases with molecular materials, the optimum light wavelength of the photoconductivity to the incident light is easily adjusted with replacement of function molecules. This is an advantage for the use of molecular materials in future applications of spintronics over the use of inorganic materials. Of course, some inorganic semiconductors show photoconductivity, while the optimum light wavelength for the photoconductivity is hard to be adjusted. Thus, for aiming to realize the control of spin current with visible light irradiation, the spin transport mechanism in molecular materials must be understood, and a number of studies of the spin transport in various molecular materials are necessary to clarify the mechanism.

At the beginning of molecular spintronics research history, the spin injection into molecular materials was performed by using a spin-polarized charge current.⁵⁻⁷ Then, some significant studies were reported by using a spin-polarized charge current.^{8,9} Meanwhile, there is a

conductance mismatch problem between a ferromagnetic material as a spin injector and a molecular material,^{10,11} which causes lowering the spin injection efficiency due to the low conductivity in molecular materials. In other words, to inject spins into molecular materials with a spin-polarized current is hard, in general.

In 2014, the spin transport in the conductive polymer PBTTT films was performed with the spin pumping and the inverse spin Hall effect (ISHE).¹² In the spin injection with the spin pumping, which is a dynamical spin injection method and generally induced with the ferromagnetic resonance (FMR) of the ferromagnetic materials,^{13,14} the conductance mismatch problem^{10,11} is thought to be negligible.¹⁵⁻¹⁸ The ISHE is a conversion effect from a spin current into a charge current via the spin-orbit interaction in the material,^{19,20} which is used as a spin current detector. Starting with the report,¹² the combination method with the spin pumping and the ISHE became to be widely used for the spin transport studies not only in polymer material films prepared by solution process,^{21,22} but also in “low-molecular-weight” molecular material films prepared by thermal evaporation.²³⁻²⁸ The spin transport in molecular materials whose carrier density is small is thought to be mainly due to polarons,¹² while the detailed of the spin transport mechanism in molecular materials is still unclear. One of the reasons to be still unclear is the lack of experimental data of the spin transport in molecular materials. Therefore, the spin transport properties in thin films of typical molecular materials should be investigated more.

In this study, a naphthyl diamine derivative (*N,N'*-Bis(naphthalen-1-yl)-*N,N'*-bis(phenyl)-2,2'-dimethylbenzidine: α -NPD) molecular thin film which is well-known as a hole transporting layer of organic light-emitting devices (OLEDs)^{29,30} is focused. An α -NPD thin film is easily prepared by thermal evaporation in vacuum. An α -NPD film is a *p*-type semiconductor and shows photoconductivity for visible light, where the spin transport properties of α -NPD films can be controlled through light irradiation. We demonstrate the spin transport in an α -NPD thin film by

using the spin pumping and the ISHE. The estimated spin diffusion length (λ) in α -NPD films is about 62 nm at room temperature (RT), which is relatively long among the “low-molecular-weight” molecular material films.

Our sample structure and experimental set up is illustrated in Figure 1. Spin transport in an α -NPD film is observed as follows: in a palladium(Pd)/evaporated- α -NPD/ $\text{Ni}_{80}\text{Fe}_{20}$ tri-layer structure sample, a spin-pump-induced pure spin current (J_s) driven by the FMR of the $\text{Ni}_{80}\text{Fe}_{20}$ film is generated in the α -NPD layer. This J_s is then absorbed into the Pd layer. The absorbed J_s is converted into a charge current as a result of the ISHE in Pd and detected as an electromotive force (E),^{12,16-19,21-28,31,32} which is expressed as,

$$\vec{E} \propto \theta_{\text{SHE}} \vec{J}_s \times \vec{\sigma} \quad , \quad (1)$$

where θ_{SHE} is the spin-Hall angle which is the conversion efficiency from a spin current to a charge current, and σ is the spin-polarization vector of the J_s . That is, if electromotive force (EMF) due to the ISHE in Pd is detected under the FMR of $\text{Ni}_{80}\text{Fe}_{20}$, it is clear evidence for spin transport in an α -NPD film.

Electron beam (EB) deposition was used to deposit Pd (Furuuchi Chemical Co., Ltd., 99.99% purity) to a thickness of 10 nm on a thermally-oxidized silicon (Si/SiO₂) substrate, under a vacuum pressure of $<10^{-6}$ Pa. Next, also under a vacuum pressure of $<10^{-6}$ Pa, α -NPD molecules (Tokyo Chemical Industry Co., Ltd.; sublimed grade) were thermally-evaporated through a shadow mask. The deposition rate and the substrate temperature during α -NPD depositions were set to 0.1 nm/s and atmospheric temperature, respectively. The α -NPD layer thickness (d) was varied between 25 and 100 nm. Finally, $\text{Ni}_{80}\text{Fe}_{20}$ (Kojundo Chemical Lab. Co., Ltd., 99.99%) was deposited by EB deposition through another shadow mask, under a vacuum pressure of $<10^{-6}$ Pa. During $\text{Ni}_{80}\text{Fe}_{20}$ deposition, the sample substrate was cooled with a cooling medium of -2°C , to

prevent the deposited molecular films from breaking. As a control experiment, samples with a Cu layer instead of the Pd layer were prepared.

An x-ray diffraction (XRD) spectrometer (Rigaku, Ultima IV) to evaluate an α -NPD film structure was used. The x-ray wavelength was 0.154 nm (Cu-K α) and a conventional out-of-plane scan was implemented. A microwave TE₀₁₁-mode cavity in an electron spin resonance (ESR) system (JEOL, JES-TE300) to excite FMR in Ni₈₀Fe₂₀, and a nano-voltmeter (Keithley Instruments, 2182A) to detect EMFs generated in the samples were used. Leading wires for detecting the output voltage properties were directly attached with silver paste at both ends of the Pd (or Cu) layer. All of the measurements were performed at RT.

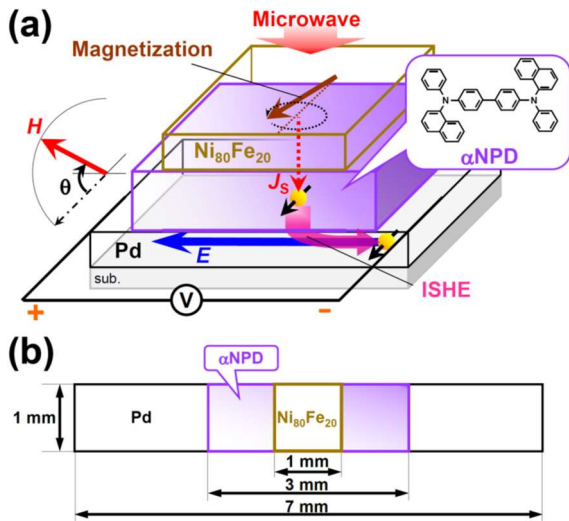


FIG. 1. (a) Bird's-eye-view and (b) top-view illustrations of our sample and orientations of external applied magnetic field (H) used in the experiments. J_s and E correspond, respectively, to the spin current generated in the α -NPD film by the spin pumping and the electromotive forces due to the ISHE in Pd.

Figure 2 shows XRD spectra of α -NPD films formed on a Pd film (10 nm in thick). θ is the incident X-ray beam angle to the sample film plane. The diffraction peaks in the range between

2θ of 31° and 37° are derived from the Si/SiO₂ substrates. We compared the α -NPD film thickness difference (50 or 100 nm) and an only Pd film. The diffraction signals near 2θ of 40° is derived from the Pd layer. No clear peaks from α -NPD films were observed. Thus, the α -NPD molecules in our samples are hardly oriented. It is indicated our α -NPD films are amorphous-like which is consistent with general α -NPD films prepared by thermal evaporation.³³

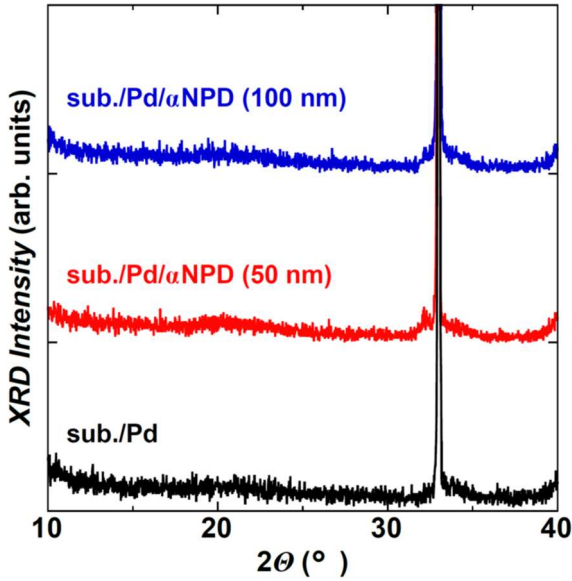


FIG. 2. X-ray diffraction spectra for α -NPD films prepared by various conditions: substrate(sub.)/Pd(10 nm in thick)/ α -NPD(100 nm), sub./Pd(10 nm)/ α -NPD(50 nm), and sub./Pd(10 nm) (without an α -NPD layer). θ is the incident x-ray beam angle to the sample film plane. The diffraction peaks in the range between 2θ of 31° and 37° are derived from the Si/SiO₂ substrates.

Figure 3(a) shows the FMR spectrum of a sample with a Pd layer and with the d of 50 nm at an external magnetic field orientation angle (θ) to the sample film plane of 0° . The applied microwave power (P) is 200 mW. H is the strength of the external static magnetic field. The FMR field (H_{FMR}) of the Ni₈₀Fe₂₀ film is 965 Oe at a microwave frequency (f) of 9.45 GHz. Thus, the

$4\pi M_S$ of the $\text{Ni}_{80}\text{Fe}_{20}$, where M_S is the saturation magnetization of the $\text{Ni}_{80}\text{Fe}_{20}$ film, is estimated to be 9,747 G with the FMR conditions in the in-plane field:

$$\frac{\omega}{\gamma} = \sqrt{H_{FMR}(H_{FMR} + 4\pi M_S)}, \quad (2)$$

where ω and γ are the angular frequency ($2\pi f$) and the gyromagnetic ratio of $1.86 \times 10^7 \text{ G}^{-1}\text{s}^{-1}$ of $\text{Ni}_{80}\text{Fe}_{20}$, respectively.^{16,24,28,32} Fig. 3(b) shows the output voltage properties of the same sample as used in Fig. 3(a); the circles represent experimental data and the solid lines are the curve fit obtained using the equation^{16,19,24,28,32}:

$$V(H) = V_{Sym} \frac{\Gamma^2}{(H-H_{FMR})^2 + \Gamma^2} + V_{Asym} \frac{-2\Gamma(H-H_{FMR})}{(H-H_{FMR})^2 + \Gamma^2}, \quad (3)$$

where Γ denotes the damping constant (22 Oe in this study). The first and second terms in eq. (3) correspond to the symmetry term to H due to the ISHE, and the asymmetry term to H due to the anomalous Hall effect and/or other effects showing the same asymmetric voltage behavior relative to the H , respectively.^{16,19,24,28,32} V_{Sym} and V_{Asym} correspond to the coefficients of the first and second terms in eq. (3), respectively. In the Fig. 3(b), output voltages from the sample are observed at the H_{FMR} at the θ of 0° and 180° . Notably, the output voltage changes their signs between the θ of 0° and 180° . This sign inversion of voltage in Pd associated with the magnetization reversal in $\text{Ni}_{80}\text{Fe}_{20}$ is characteristic of the ISHE.^{16,19,24,28,32}

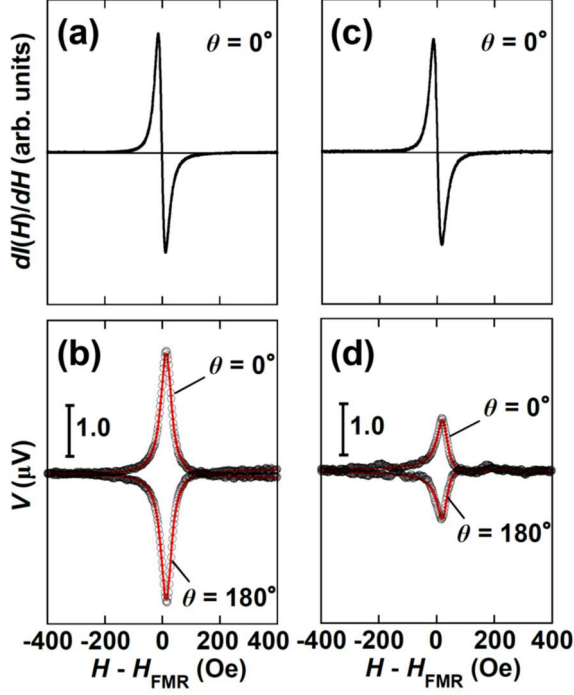


FIG. 3. (a) FMR spectrum and (b) output voltage properties of a sample with a Pd layer. (c) FMR spectrum and (d) output voltage properties of a sample with a Cu layer. θ is the static magnetic field (H) angle to the sample film plane. H_{FMR} is the ferromagnetic resonance field. The α -NPD film thickness is 50 nm and the applied microwave power is 200 mW.

As a control experiment, we tested samples with a Cu layer instead of the Pd layer. Fig. 3(c) shows the FMR spectrum of a sample with a Cu layer and with the d of 50 nm at the θ of 0° . The P is 200 mW. Fig. 3(d) shows output voltage properties of the same sample as used in Fig. 3(c), where EMFs were also observed at the θ of 0° and 180° . The EMFs observed from the sample with a Cu layer was less than a half of those from the sample with a Pd layer as shown in Fig. 3(b). As long as compared the θ_{SHE} difference between Pd and Cu due to the spin-orbit interaction difference, the EMFs in Fig. 3(d) may be large. There is a possibility that the surface of the Cu layer is naturally-oxidized in the sample making process because a naturally-oxidized Cu thin film show the ISHE.³⁴ Thus, it is no wonder that certain EMFs are observed from a sample

with a Cu layer. A similar trend is seen even in a previous report with a Cu/molecular-film/ $\text{Ni}_{80}\text{Fe}_{20}$ tri-layer structure.²⁸ Eventually, the EMFs observed from a sample with a Pd layer is large enough compared with that from a sample with a Cu layer. As another control experiment, we studied the P dependence of the EMFs in a sample with a Pd layer and with the d of 50 nm at the θ of 0° ; the results are shown in Fig. 4. The V_{Sym} linearly increases with the P . The above results suggest that the dominant origin of the EMF at the H_{FMR} observed from the sample with a Pd layer (see Fig. 3(b)) is due to the ISHE in Pd. That is, the spin transport in an evaporated α -NPD film driven by the spin-pumping has been achieved at RT.

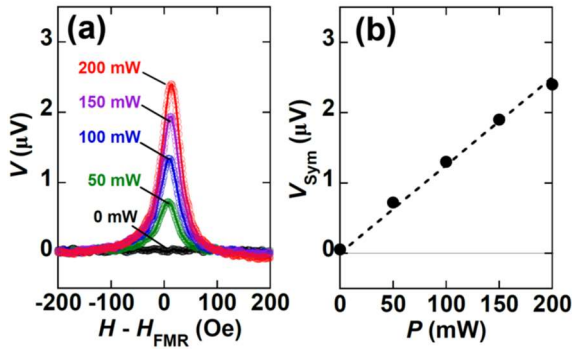


FIG. 4. (a) Microwave power (P) dependence of electromotive forces generated in a sample with the α -NPD film thickness of 50 nm and (b) an analysis result obtained with eq. (3). V_{Sym} corresponds to the coefficient of the first term in eq. (3). The dashed line in (b) is a linear fit.

Figure 5 shows the d dependences of (a) $4\pi M_S$ in samples calculated via eq. (2) and of (b) V_{Sym} estimated via eq. (3). Circles are the experimental data. With increasing d , V_{Sym} due to the ISHE in Pd seems to decrease with large deviation while M_S slightly decreases. The same tendency about the V_{Sym} with large deviation has been observed in previous studies,^{24,28} and there is no correlation between the V_{Sym} deviation and the experimental setup which is the Q-factor for the ESR cavity, the sample setting methods, the measurement temperature, and so on. One

possible reason of the V_{Sym} deviation may be due to random networks of π -electron orbit in α -NPD films originating from the amorphous-like structure. Hence, similarly to the previous studies,²⁸ we estimated the λ in α -NPD films with deviation, as follows: Two fitting curves for the λ evaluation in α -NPD films with estimation deviation were drawn as shown in the dashed lines in Fig. 5(b), under an assumption of an exponential decay of the spin current in α -NPD films which means the spin current in α -NPD films is diffusive: One is the fit for the longest λ (~ 80 nm) by using relatively-small value data set. Another is the fit for the shortest λ (~ 44 nm) by using relatively-large value data set. Almost data was inside of these to dashed lines. Therefore, using the center value and the range between the longest and shortest values, the λ in α -NPD films was estimated to be 62 ± 18 nm at RT.

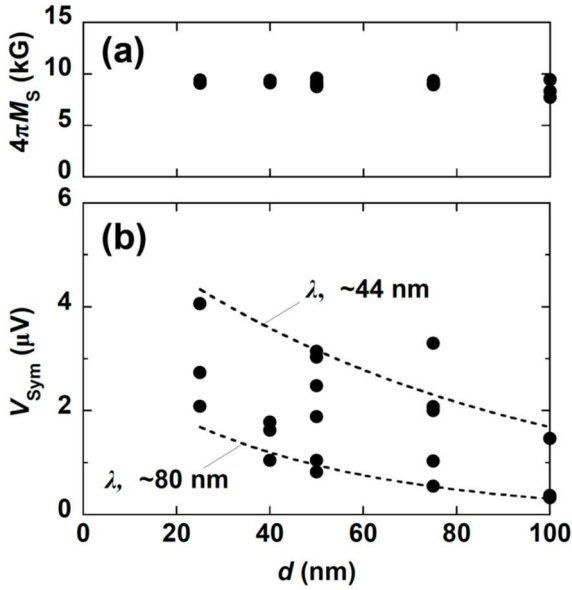


FIG. 5. Dependences of (a) $4\pi M_S$ (M_S : saturation magnetization), calculated via eq. (2), and of (b) V_{Sym} estimated by eq. (3), on the α -NPD film thickness (d). Circles are the experimental data. The dashed lines in (b) are curve fits under an assumption of an exponential decay of the spin current in α -NPD films.

We discuss the validity of the λ estimation of our α -NPD films with the reported values in other molecular materials studied by using a spin-pump-induced spin current.^{11,12,21,23,24,26-28,31} The estimated λ of 62 ± 18 nm in an α -NPD film at RT is comparable or relatively long value among the reported spin diffusion lengths of other “low-molecular-weight” molecular films prepared by thermal evaporation: ~ 13 nm for C_{60} fullerene,³¹ ~ 14 nm for PTCDA,²⁸ ~ 25 nm for C_{84} fullerene,³¹ ~ 35 nm for TIPS-pentacene,²⁶ ~ 42 nm for “normal” pentacene,²⁴ ~ 50 nm for Alq_3 ,²³ and ~ 132 nm for rubrene.²⁷ Most of these reference data are for amorphous or partially-oriented molecular films. On the other hand, polymer films, such as PBTTT and PEDOT:PSS films, tend to possess longer spin diffusion lengths than “low-molecular-weight” molecular films: ~ 140 nm for PEDOT:PSS,²¹ and ~ 200 nm for PBTTT.¹² A polyaniline film, which is a conductive polymer film, has an extremely long spin diffusion length of ~ 590 nm at RT.¹¹ The relationship between the molecular orientation and the spin diffusion length in molecular films in those reference has not been studied yet. It is significant for developing the molecular spintronic devices to investigate its relationship in the molecular films, although the spin diffusion length of several tenth nm may be long enough for spintronic application because the recent nanotechnology has been much evolved. This relationship will be studied in near future by using the samples with molecular films having good molecular orientation. At a glance, the estimated λ of ~ 62 nm in α -NPD films is a little surprising compared to the spin diffusion length of ~ 42 nm in pentacene films²⁴ because α -NPD films in this study is amorphous-like while the pentacene molecules in the films are partially oriented.²⁴ The molecular grains of pentacene molecules in the previous study²⁴ may not be so large. That is, the average grain size in a molecular film might be significant to decide the spin diffusion length in molecular films, as similar to the case in C_{60} fullerene film investigated by a spin-polarized current.⁹ The grain boundary of molecular grains in films might be a significant factor of the spin

scattering in the spin transport. Also, in a pentacene single crystal, there is anisotropy of conductivity due to the molecular orientation. In other words, molecular oriented pentacene films must show long spin diffusion length in a specific crystal orientation, which is the π -electron orbital may be well-connected between inter-molecules. Meanwhile, for an α -NPD film, the spin transport may be isotropic because α -NPD films make amorphous generally and automatically, where the π -orbital makes random network. This is convenient for industry because if α -NPD films are used as a spin transporting material in devices, the device characteristics will be stable. Finally, the reason why the evaporated rubrene films show such a long spin diffusion length of ~ 132 nm is unknown because the electrical conductivity in the thermally-evaporated rubrene films is low compared with pentacene films prepared by thermal evaporation, although the rubrene single-crystal based thin film transistor shows the best performance among molecular materials.³⁵ The spin transport mechanism due to polarons may be quite different from the spin transport due to “normal” carriers (electrons or holes).

In summary, spin transport properties of thermally evaporated α -NPD films were studied at RT by using the spin pumping for spin injection and using the ISHE in non-magnetic metals for the spin detection methods. We achieved spin transport in evaporated α -NPD films; the spin diffusion length in α -NPD was estimated to be about 62 nm at RT, which is long enough to utilize as a spin transport material for future spintronic devices.

This research was partly supported by the Grant-in-Aid from the Japan Society for the Promotion of Science (JSPS) for Scientific Research (B) (No. 20H02715) (to Y. T and E. S.), and by the Cooperative Research Program of “Network Joint Research Center for Materials and Devices” (to E. S.).

References:

- ¹T. Suzuki, T. Sasaki, T. Oikawa, M. Shiraishi, Y. Suzuki, and K. Noguchi, *Appl. Phys. Exp.* **4**, 023003 (2011).
- ²T. Tahara, H. Koike, M. Kamenno, T. Sasaki, Y. Ando, K. Tanaka, S. Miwa, Y. Suzuki, and M. Shiraishi, *Appl. Phys. Exp.* **8**, 113004 (2015).
- ³S. Sugahara, and M. Tanaka, *Appl. Phys. Lett.* **84**, 2307 (2004).
- ⁴O. Ostroverkhova, D. G. Cooke, S. Shcherbyna, R. F. Egerton, F. A. Hegmann, R. R. Tykwinski, and J. E. Anthony, *Phys. Rev. B* **71**, 035204 (2005).
- ⁵K. Tsukagoshi, B. W. Alphenaar, and H. Ago, *Nature* **401**, 572 (1999).
- ⁶V. Dediu, M. Murgia, F. C. Maticcotta, C. Taliani, and S. Barbanera, *Solid State Commun.* **122**, 181 (2002).
- ⁷Z. H. Xiong, D. Wu, Z. V. Vardeny, and J. Shi, *Nature* **427**, 821 (2004).
- ⁸G. Salis, S. F. Alvarado, M. Tschudy, T. Brunswiler, and R. Allenspach, *Phys. Rev. B* **70**, 085203 (2004).
- ⁹T. D. Nguyen, F. Wang, X. -G. Li, E. Ehrenfreund, and Z. V. Vardeny, *Phys Rev. B* **87**, 075205 (2013).
- ¹⁰G. Schmidt, D. Ferrand, L. W. Molenkamp, A. T. Filip, and B. J. van Wees, *Phys. Rev. B* **62**, R4790 (2000).
- ¹¹A. Fert, and H. Jaffres, *Phys. Rev. B*, **64**, 184420 (2001).
- ¹²S. Watanabe, K. Ando, K. Kang, S. Mooser, Y. Vaynzof, H. Kurebayashi, E. Saitoh, and H. Sirringhaus, *Nature Phys.* **10**, 308 (2014).
- ¹³Y. Tserkovnyak, A. Brataas, and G. E. W. Bauer, *Phys. Rev. Lett.* **88**, 117601 (2002).
- ¹⁴S. Mizukami, Y. Ando, and T. Miyazaki, *Phys. Rev. B* **66**, 104413 (2002).
- ¹⁵K. Ando, S. Takahashi, J. Ieda, H. Kurebayashi, T. Trypiniotis, C.H.W. Barnes, S. Maekawa,

- and E. Saitoh, *Nature Mater.*, **10**, 655 (2011).
- ¹⁶E. Shikoh, K. Ando, K. Kubo, E. Saitoh, T. Shinjo, and M. Shiraishi, *Phys. Rev. Lett.* **110**, 127201 (2013).
- ¹⁷M. Koike, E. Shikoh, Y. Ando, T. Shinjo, S. Yamada, K. Hamaya, and M. Shiraishi, *Appl. Phys. Exp.* **6**, 023001 (2013).
- ¹⁸Z. Tang, E. Shikoh, H. Ago, K. Kawahara, Y. Ando, T. Shinjo, and M. Shiraishi, *Phys. Rev. B* **87**, 140401 (2013).
- ¹⁹E. Saitoh, M. Ueda, H. Miyajima, and G. Tatara, *Appl. Phys. Lett.* **88**, 182509 (2006).
- ²⁰S. O. Valenzuela, and M. Tinkham, *Nature* **442**, 176 (2006).
- ²¹M. Kimata, D. Nozaki, Y. Niimi, H. Tajima, and Y. Otani, *Phys. Rev. B* **91**, 224422 (2015).
- ²²J. B. S. Mendes, O. A. Santos, J. P. Gomes, H. S. Assis, J. F. Felix, R. L. Rodriguez-Suarez, S. M. Rezende, and A. Azevedo, *Phys. Rev. B* **95**, 014413 (2017).
- ²³S. W. Jiang, S. Liu, P. Wang, Z. Z. Luan, X. D. Tao, H. F. Ding, and D. Wu, *Phys. Rev. Lett.* **115**, 086601 (2015).
- ²⁴Y. Tani, Y. Teki, and E. Shikoh, *Appl. Phys. Lett.* **107**, 242406 (2015).
- ²⁵Y. Tani, T. Kondo, Y. Teki, and E. Shikoh, *Appl. Phys. Lett.* **110**, 032403 (2017).
- ²⁶Y. Tanaka, T. Kono, Y. Teki, and E. Shikoh, *IEEE Trans. Magnetics* **55**, 1400304 (2019).
- ²⁷Z. Li, T. Li, D. -C. Qi, W. Tong, L. Xu, J. Zhu, Z. Zhang, H. Xu, W. Zhang, Y. Guo, F. Chen, Y. Han, L. Cao, F. Zhang, and Y. Xiong, *Appl. Phys. Lett.* **115**, 053301(2019).
- ²⁸K. Nishida, Y. Teki, and E. Shikoh, *Solid State Commun.* **312**, 113898(2020).
- ²⁹S. A. Van Slyke, C. H. Chen and C. W. Tang, *Appl. Phys. Lett.* **69**, 2160 (1996).
- ³⁰J. Shi, and C. W. Tang, *Appl. Phys. Lett.* **70**, 1665 (1997).
- ³¹H. Liu, J. Wang, A. Chanana, and Z. V. Vardeny, *J. Appl. Phys.* **125**, 142908 (2019).
- ³²K. Ando, and E. Saitoh, *J. Appl. Phys.* **108**, 113925 (2010).

³³F. Suzuki, S. Kubo, T. Fukushima, and H. Kaji, *Sci. Rep.* **8**, 5203 (2018).

³⁴H. An, Y. Kageyama, Y. Kanno, N. Enishi, and K. Ando, *Nature Commun.* **7**, 13069 (2016).

³⁵J. Takeya, M. Yamagishi, Y. Tominari, R. Hirahara, Y. Nakazawa, T. Nishikawa, T. Kawase, T. Shimoda, and S. Ogawa, *Appl. Phys. Lett.* **90**, 102120 (2007).